Journal of Applied Electrochemistry **32**: 179–184, 2002.

Electrochemical behaviour of Ni + Al alloy as an alternative material for molten carbonate fuel cell cathodes

T. KUDO[1]*, Y. HISAMITSU[2], K. KIHARA[2], M. MOHAMEDI[2] and I. UCHIDA[3]
[1]*Research and Development Center, Tohoku Electric Power Co. Inc., 7-2-1 Nakayama, Aoba-ward, Sendai 981-0952, Japan*
[2]*Department of Applied Chemistry, Graduate School of Engineering, Tohoku University, 07 Aramaki-Aoba, Aoba-ward, Sendai 980-8579, Japan*
[3]*New Industry Creation Hatchery Center, Tohoku University, 04 Aramaki-Aoba, Aoba-ward, Sendai-city, Miyagi 980-8579, Japan*
*(*author for correspondence, e-mail: tkudo@rdc.tohoku-epco.co.jp)*

Received 23 January 2001; accepted in revised form 5 November 2001

Key words: cathode material, fractal, MCFC, molten carbonate, Ni + Al alloy

Abstract

This paper presents an investigation of the performance and stability for oxygen reduction on *in situ* oxidized Ni alloys, specially focused on 95 at % Ni + 5 at % Al and 85 at % Ni + 15 at % Al alloy electrodes in Li/Na carbonate eutectic. Test specimens of the alloys were prepared as thin film electrodes sputtered onto Au substrates. *In situ* oxidation of alloy electrodes and electrochemical measurements for oxygen reduction on the electrodes were performed in the free-volume melt at 923 K. It was found that the *in situ* oxidized Ni + Al alloys exhibit higher performance for the oxygen reduction than the NiO without Al. Electrochemical fractal analysis (EFA) revealed higher oxide film stability of the Ni + Al alloys in comparison to NiO electrodes. The surface morphology of the alloy specimen after oxidation was investigated with SEM and AFM.

1. Introduction

Internal short-circuiting due to the dissolution of the NiO cathode is commonly recognized as one of the most serious issues limiting the life span of molten carbonate fuel cells (MCFC). Thus, alternative materials (e.g., $LiCoO_2$, NiO supplemented with MgO or Fe_2O_3, or NiO coated with $LiCoO_2$) have been developed to lower the solubility of the cathode [1]. From this viewpoint, we have carried out investigations on oxygen reduction on *in situ* oxidized metals (e.g., NiO, $LiCoO_2$ and Li_2MnO_3) in carbonate melt [2–11]. In this article, we describe the electrochemical behavior of 95 at % Ni + 5 at % Al and 85 at % Ni + 15 at % Al alloys for oxygen reduction in Li/Na carbonate eutectic.

In the MCFC field, Al has been used as the corrosion protective layer for the wet seal [12, 13]. The elements coated with Al oxides are resistive against the attack by molten carbonate. However, Al oxide layer exhibits a high electrical resistance; thus little attention has been given to apply Al as an additive for NiO cathodes, which must provide sufficient electric conductivity. We expect that a certain Ni content in the alloy improves the conductivity of Ni + Al oxides, which are still stable in the molten carbonate because of the protective effect of Al. It is also expected that $LiAl_yNi_{1-y}O_2$ might be involved in the *in situ* alloy oxidation process. The synthesis of $LiAl_yNi_{1-y}O_2$ has been already achieved for $y \leqslant 0.3$ and it was shown by X-ray diffraction that the Ni is substituted by Al when $y \leqslant 0.2$ [14].

In this work, thin films of Ni + Al alloys were prepared on gold substrates by a sputtering method and oxidized in carbonate melt at 923 K. The oxidized products were then tested as working electrodes for oxygen reduction in the melt. There are several studies on oxidation of Ni + Al alloys in gas phases [15] and in molten Na_2CO_3 at 1273 K [16], since Ni + Al alloys are superalloys usable in oxidative atmospheres at high temperatures. Therefore, the oxidation behaviour and surface morphology of the Ni + Al alloys are of some interest as also is the kinetic behavior of oxygen reduction on *in situ* formed oxides. Voltammetric behaviours of Ni + Al oxides are compared with pure Ni to show that Ni + Al alloy with low Al content is electrochemically active and stable in the carbonate melt.

2. Experimental details

Electrochemical measurements were performed with electrodes consisting of a thin layer of Ni + Al alloy

sputtered onto both sides of a gold flag of 0.39 cm^2 geometrical area. Alloys of two compositions, 95 at % Ni + 5 at % Al, 85 at % Ni + 15 at % Al, and pure Ni were tested. These samples will be denoted as Ni + 5 Al/Au, Ni + 15 Al/Au, and Ni/Au, respectively. The thickness of the sputtered sample was 0.75 μm. An Anelva L-350S-C equipped with targets of the same composition as the desired alloy was used for sputtering. The procedures for melt purification, gas handling, temperature control, and cell assembly including the counter electrode are described in previous work [2, 3, 6]. In this work, a gold flag was used as quasi-reference electrode. However, all electrochemical potentials are reported against the standard Au | (O_2:CO_2 = 0.33:0.67 atm) gas reference electrode (SOE). The three samples mentioned above were immersed in the $(Li_{0.52}Na_{0.48})_2CO_3$ eutectic saturated with a 0.9 atm O_2 + 0.1 atm CO_2 atmosphere at 923 K at the same time, and were subjected to *in situ* oxidation simultaneously. In addition, the samples were quickly immersed into the melt without annealing to prevent alloying of the gold substrate with Ni + Al alloys. The open circuit potential and the a.c. impedance at 1 kHz were simultaneously recorded during the oxidation process according to the procedure reported elsewhere [3].

The phase distribution and lattice parameter of the oxides were characterized with a Rigaku RINT-2500 X-ray diffractometer (XRD) equipped with a thin film rotating sample holder using Cu$K\alpha$ radiation. The 2θ scan mode with an incident angle of two degrees was employed to obtain thin film XRD profiles. The surface morphology of the oxides was observed by using a Jeol JSM-5310LV scanning electron microscope (SEM) and a Digital Instruments NanoScope IIIa Dimension3000 atomic force microscope (AFM). The cathodic performance and stability of the oxides were evaluated by linear sweep voltammetry (LSV) and the variation in peak current density (j_p) of LSV with time, respectively, under the same condition mentioned above. A Solartron 1286 potentiostat and a homemade potential sweeper were used for the measurements. All electrochemical measurements were carried out under fully immersed conditions, thus all electrochemical data were obtained under semiinfinite diffusion control.

3. Results and discussion

Figure 1 shows a variation in the open circuit potential (o.c.p.) and the film resistance (R_S) of Ni + 15Al/Au with time. R_S is the real part of the film impedance recorded at 1 kHz. The change in o.c.p. and R_S shows four regions denoted as A, B, C, and D in Figure 1. It should be noted that the initial cathodic shift in O.C.P at an earlier stage of oxidation (region A) is unique to the Ni + Al alloys. Such a phenomenon has not been observed during the oxidation of Ni and Co [3, 4, 10, 11]. Pure Ni exhibits −0.76 V vs SOE just after immersion [6, 11]. This may indicate that the Al in the alloy had been oxidized before immersion, forming a kind of passivation layer, which shows a more anodic potential than the unoxidized Ni. This layer was then destroyed just after the immersion. Thus, temporary exposure of fresh surface of the alloy resulted in the cathodic shift of the o.c.p. The oxidation and lithiation processes after the region B are almost similar to the case of Ni [6, 11]. It took about 9000 s to complete the oxidation of Ni + 15Al/Au. The R_s value after complete oxidation (0.2 Ω cm^2) is almost the same order of magnitude as that of lithiated NiO [3, 11] and low enough to be subjected to electrochemical measurements.

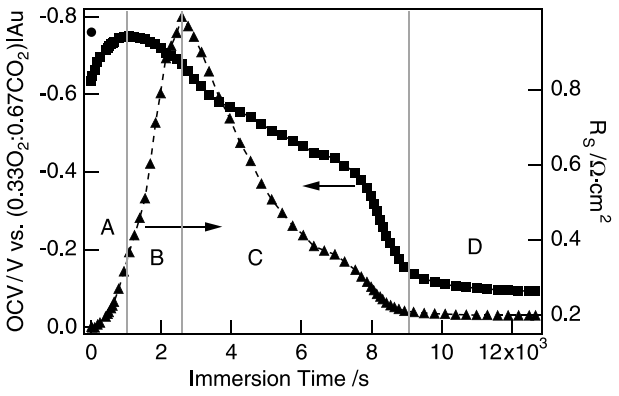

Fig. 1. Variation in open circuit potential (OCP) and film resistance (R_S) with time during *in situ* oxidation of Ni + 15Al/Au under P_{O_2}/P_{CO_2} = 0.9/0.1 atm in $(Li_{0.53}Na_{0.47})_2CO_3$ at 923 K. Circular marker shows the o.c.p. of pure Ni just after immersion. Key: (■) o.c.p.; (▲) R_S; (●) pure Ni.

Oxidation products characterized by thin film XRD are shown in Figure 2. No Al related phase, such as α-Al_2O_3 (space group $R\bar{3}c$) or α-$LiAlO_2$ (space group $R\bar{3}m$), other than NiO (space group $Fm\bar{3}m$) was observed. The lattice parameter was calculated from the XRD profiles in the cubic setting. The deviation of peak position from the intrinsic one was compensated against the peaks of the gold substrate, which was exploited as an internal standard material. We adopted 0.407 86 nm as the cubic lattice parameter of Au (JCPDS no. 4-784). The linear decrease in lattice parameter with Al content (see Figure 3) indicates that the Ni + Al alloys formed a solid solution by *in situ* oxidation. This agrees with the fact that the ionic radius of Al^{3+} is smaller than that of Ni^{3+} (53.5 pm and 56 pm, respectively in VI-coordinate [17]). The intensity of the peaks attributed to NiO decreased with increasing Al content. On the other hand, the intensity of the gold substrate increased. This suggests that the oxide layer of Ni + Al/Au was thinned by dissolution or exfoliation.

Figure 4 shows linear sweep voltammograms (LSV) for oxygen reduction on (a) Ni + 15Al/Au, (b) Ni + 5Al/Au, (c) Ni/Au, and (d) on bare gold substrate. These curves were recorded at a sweep rate of 0.2 V s^{-1} just after completing the oxidation. Higher currents per apparent electrode area of Ni + Al alloys than that of

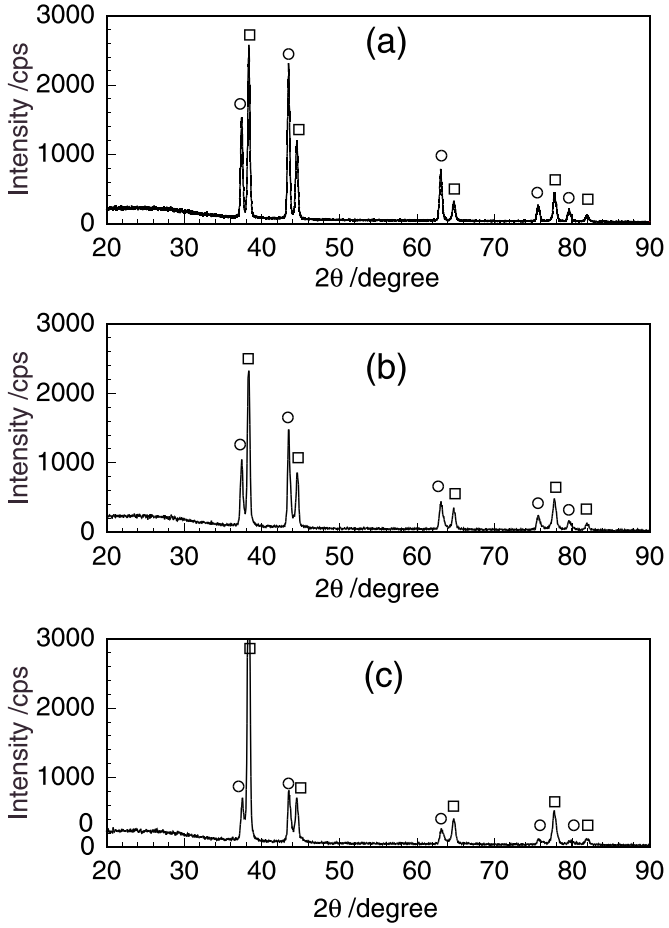

Fig. 2. Thin film X-ray diffraction profiles of oxidation products, which were obtained under $P_{O_2}/P_{CO_2} = 0.9/0.1$ atm in $(Li_{0.53}Na_{0.47})_2CO_3$ at 923 K: (a) Ni/Au, (b) Ni + 5Al/Au, (c) Ni + 15Al/Au. Key: (○) NiO; (□) Au.

NiO were clearly demonstrated in Figure 4. The stability of each sample, evaluated from the decrease in peak current density (j_p) of LSV with time, is presented in Figure 5. The j_p measured at the same potential with that of the j_p for gold are compared. The Ni + Al alloys are superior to the NiO within the time domain of the measurements. This seems to contradict the explanation provided from the XRD profiles (Figure 2), indicating deterioration of the oxide layer. For further investigation, the surface morphology of each sample was observed by SEM and AFM. Figure 6 and Figure 7

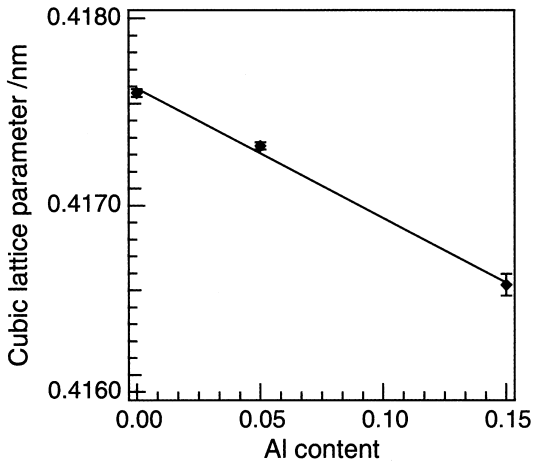

Fig. 3. Correlation between Al content and lattice parameter of oxidized Ni + Al/Au surface in cubic setting.

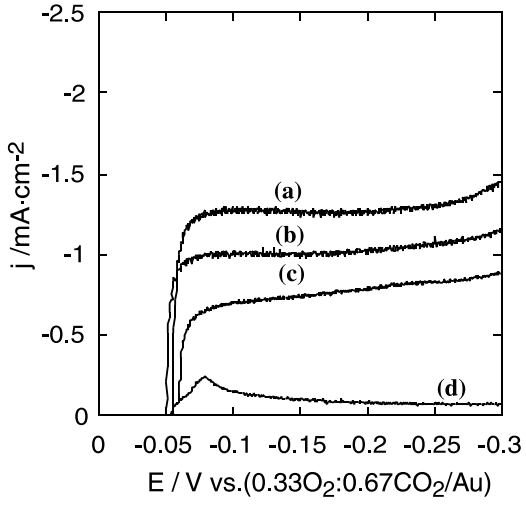

Fig. 4. Linear sweep voltammograms for oxygen reduction on oxidized Ni + Al/Au electrodes under $P_{O_2}/P_{CO_2} = 0.9/0.1$ atm in $(Li_{0.53}Na_{0.47})_2CO_3$ at 923 K, sweep rate 0.2 V s^{-1}. Key: (a) Ni + 15 Al/Au; (b) Ni + 5 Al/Au; (c) Ni/Au; (d) bare Au.

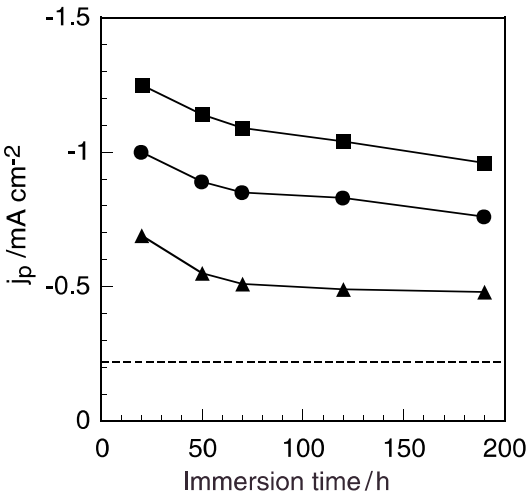

Fig. 5. Effect of immersion time on the peak current density j_p for oxygen reduction on oxidized Ni/Al electrodes under $P_{O_2}/P_{CO_2} = 0.9/0.1$ atm in $(Li_{0.53}Na_{0.47})_2CO_3$ at 923 K, sweep rate 0.2 V s^{-1}. Key: (■) Ni + 15 Al/Au; (●) Ni + 5 Al/Au; (▲) Ni/Au; (- - -) bare Au.

show the SEM and AFM images of the surface of each sample taken just after completion of oxidation. As can be seen in Figure 6, the oxide surface of Ni + 15Al/Au exhibits characteristic morphology, that is octahedral particles of about two micrometers in size. The surface roughness r.m.s. (root mean square) calculated from AFM (Figure 7) is 755, 455 and 295 nm for Ni + 15Al/Au, Ni + 5Al/Au and Ni/Au, respectively. Higher surface irregularity of the Ni + 15Al/Au will probably result in a higher j_p value in the LSV in comparison to the other oxides.

For such a surface irregularity of the electrode under diffusion control, electrochemical fractal analysis (EFA) is an effective technique [18, 19]. If the dependence of log (*area*) on log (*characteristic length*) is approximately linear over a certain range, then the surface can be regarded as fractal in this range, otherwise the fractal approximation is denied. The oxygen reduction at NiO and Ni + Al oxides in molten carbonate would fulfill conditions required for EFA for the following reasons: (i) The charge transfer rate is high [20]; (ii) the electrolyte is an ionic melt, hence its resistance is negligibly low; (iii) the interface is planar; and in the effects of migration and convection can be neglected within the time scale of this experiment. Thus, the EFA was applied to explain the stability of Ni + Al oxide electrodes based on the peak current density of the LSV.

When the overall rate of the reaction is controlled by diffusion and the electrode is smooth and planar, LSV peak current j_p is proportional to the square root of the scan rate v (Randles–Sevcik equation). For fractal (rough) electrodes, this relationship is no longer valid and j_p is proportional to v^α ($\alpha \neq 0.5$) rather than $v^{0.5}$ [18, 19]. So that, j_p on the rough electrode is given by

$$j_p = Av^\alpha \tag{1}$$

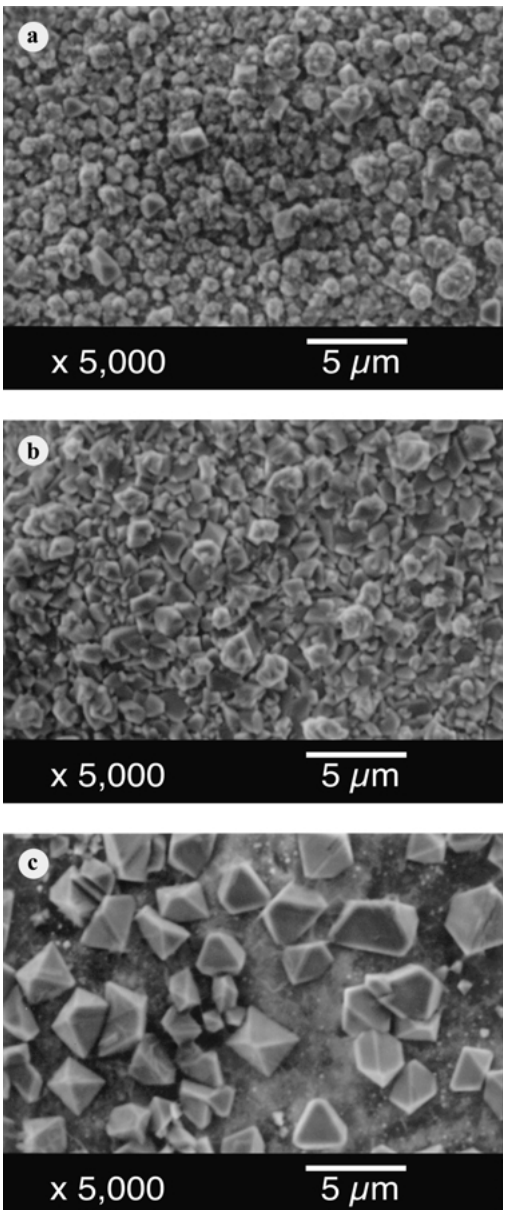

Fig. 6. Scanning electron microscopic images of oxide surface taken just after oxidation: (a) Ni/Au, (b) Ni + 5Al/Au; (c) Ni + 15Al/Au.

where A is the proportionality factor, v the scan rate, and α is directly linked with the fractal dimension D_F of the interface by the following equation [21]:

$$\alpha = \frac{D_F - 1}{2} \tag{2}$$

Generally, for conductive, corrugated, and contiguous surfaces: $3 \geqslant D_F > 2$. However, when the surface is only partially active, that is, if the surface is partially blocked, $D_F < 2$. On the other hand, D_F of a smooth electrode should be equal to 2 ($\alpha = 0.5$). Figure 8 illustrates how the D_F affects the shape of the diffusion layer. When the surface is rough enough to deform the shape of diffusion layer (Figure 8 (1)), D_F exhibits values greater than two; for a smooth surface (Figure 8 (2)), D_F is equal to two.

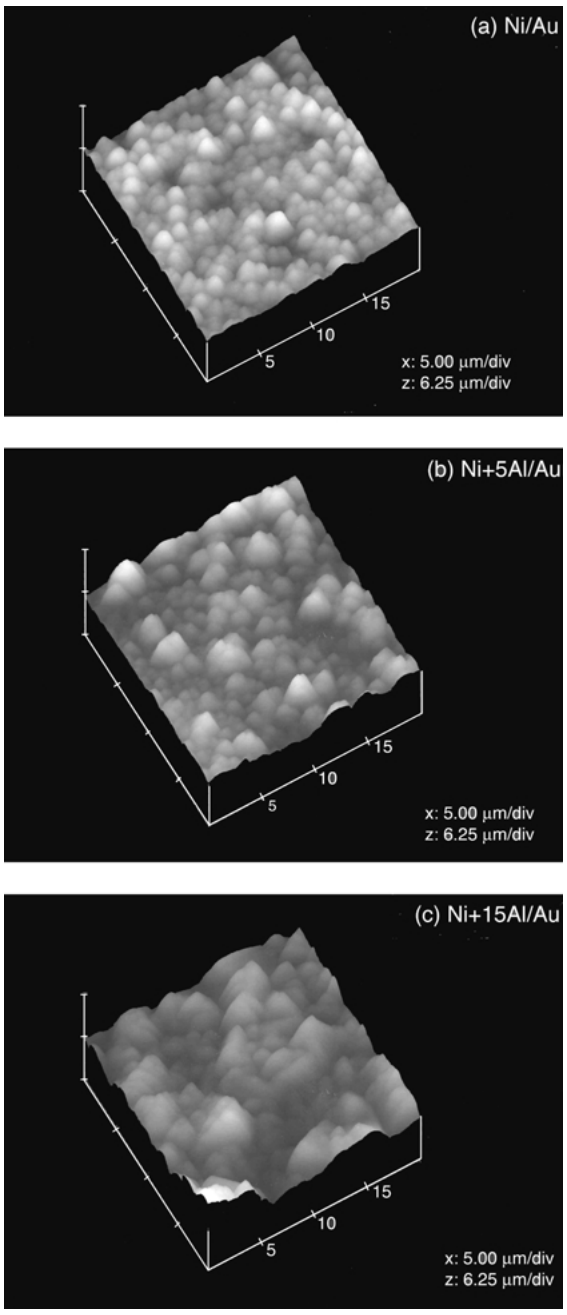

Fig. 7. Atomic force microscopic images of oxide surface taken just after oxidation: (a) Ni/Au, (b) Ni + 5Al/Au, (c) Ni + 15Al/Au.

A convenient way to evaluate the coefficient α (and D_F in Equation 2) is to plot j_p and v using a double logarithmic scale and determine the slope (α) in the linear range of the plot. For the LSV curves presented in Figure 4, the dependence of log (j_p) on log (v) is shown in Figure 9. The slope α (D_F calculated according to the Equation 2) is 0.85 ($D_F = 2.70$), 0.83 ($D_F = 2.66$), 0.80 ($D_F = 2.60$), and 0.66 ($D_F = 2.32$) for Ni + 15Al/Au, Ni + 5Al/Au, Ni/Au, and Au, respectively. This means that the Ni + Al oxide electrodes show a more irregular surface geometry in the fractal dimension sense than NiO and Au. Figure 10 shows the variation in α and D_F with time. From the viewpoint of electrochemical

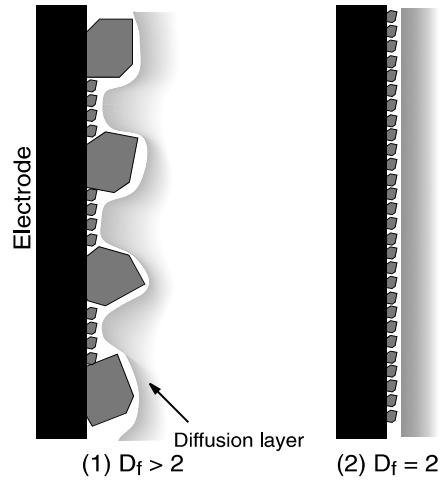

Fig. 8. Schematic illustration describing the relationship among the D_F, the surface roughness, and the shape of diffusion layer.

fractals, the surface of Ni + Al oxides remains rough even after 200 h immersion in the molten carbonate, which kept a j_p of LSV higher than that of NiO.

4. Conclusion

Ni + Al alloys oxidized in the Li/Na carbonate eutectic form solid solution type oxides, in which Ni^{3+} in the lithiated NiO is partially substituted with Al^{3+}. Ni + Al oxides were found to be electrochemically active for oxygen reduction and the peak current density of LSV on the Ni + Al oxide electrodes remained higher in comparison to NiO over 200 h. The higher performance of Ni + Al oxides may be attributed to their stabilized rough surfaces. Additionally, electrochemical fractal analysis revealed that the surface morphology of Ni + Al

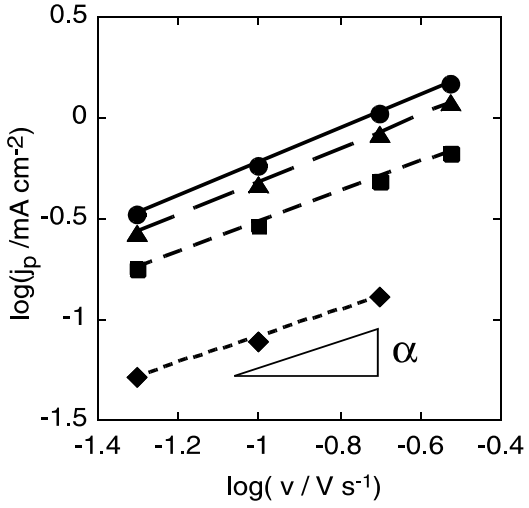

Fig. 9. Double logarithmic plots of the peak current density as a function of the sweep rate v on various electrodes under $P_{O_2}/P_{CO_2} = 0.9/0.1$ atm in $(Li_{0.53}Na_{0.47})_2CO_3$ at 923 K. Key: (●) Ni + 15 Al/Au; (▲) Ni + 5 Al/Au; (■) Ni/Au; (- - -) bare Au.

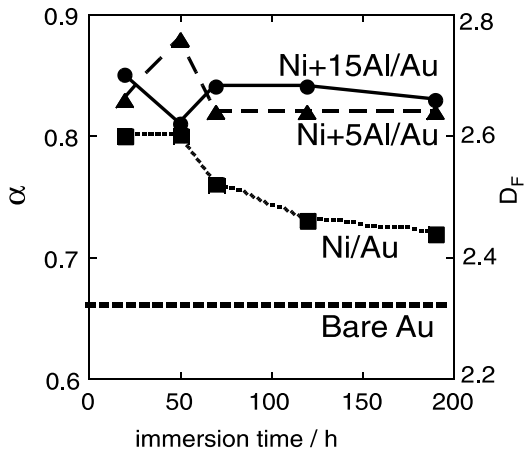

Fig. 10. Dependence of the coefficient α and the fractal dimension D_F, calculated from the peak current density of LSV curves, on the immersion time for various electrodes under $P_{O_2}/P_{CO_2} = 0.9/0.1$ atm in $(Li_{0.53}Na_{0.47})_2CO_3$ at 923 K. Key: (●) Ni + 15 Al/Au; (▲) Ni + 5 Al/Au; (■) Ni/Au; (- - -) bare Au.

oxides is more stable than that of NiO. This favors the compounds under study as candidate MCFC cathode materials.

Acknowledgement

This work was partly supported by the Proposal-Based Immediate-Effect R&D Promotion Program 98Z31-011 from the New Energy and Industrial Technology Development Organization (NEDO).

References

1. T. Fukui, H. Okawa and T. Tsunooka, *J. Power Sources* **71** (1998) 239.
2. I. Uchida, Y. Mugikura, T. Nishina and K. Itaya, *J. Electroanal. Chem.* **206** (1986) 241.
3. T. Nishina, K. Takizawa and I. Uchida, *J. Electroanal. Chem.* **263** (1989) 87.
4. K. Yamada and I. Uchida, *Chem. Lett.* (1994) 299.
5. K. Yamada and I. Uchida, *J. Electroanal. Chem.* **385** (1995) 57.
6. P. Tomczyk, H. Sato, K. Yamada, T. Nishina and I. Uchida, *J. Electroanal. Chem.* **391** (1995) 125.
7. P. Tomczyk, H. Sato, K. Yamada, T. Nishina and I. Uchida, *J. Electroanal. Chem.* **391** (1995) 133.
8. C.G. Lee, K. Yamada, T. Nishina and I. Uchida, *J. Power Sources* **62** (1996) 145.
9. K. Yamada, N. Sato, T. Fujino, M. Nishizawa and I. Uchida, *Electrochem.* **67** (1999) 68.
10. M. Mohamedi, Y. Hisamitsu, T. Kudo, T. Itoh, and I. Uchida, *J. Solid State Electrochem.* **5** (2001) 538.
11. T. Kudo, Y. Hisamitsu, K. Kihara, M. Mohamedi and I. Uchida, *J. Power Sources* **104** (2002) 272.
12. R.B. Swaroop, J.W. Sim and K. Kinoshita, *J. Electrochem. Soc.* **125** (1978) 1799.
13. N. Fujimoto, M. Yamamoto and T. Nagoya, *J. Power Sources* **71** (1998) 231.
14. T. Ohzuku, A. Ueda and M. Kouguchi, *J. Electrochem. Soc.* **142** (1995) 4033.
15. H.M. Hindam and W.W. Smeltzer, *J. Electrochem. Soc.* **127** (1980) 1622.
16. C.T. Liu and O.F. Devereux, *J. Electrochem. Soc.* **138** (1991) 3349.
17. R.D. Shannon, *Acta Cryst.* **A32** (1976) 751.
18. T. Pajkossy, *J. Electroanal. Chem.* **300** (1991) 1.
19. P. Ocon, P. Herrasti, L. Vazquez, R.C. Salvarezza, J.M. Vara and A. J. Arvia, *J. Electroanal. Chem.* **319** (1991) 101.
20. T. Nishina, I. Uchida and J.R. Selman, *J. Electrochem. Soc.* **141** (1994) 1191.
21. M.S. Mattsson, G.A. Niklasson and C.G. Granqvist, *Phys. Rev. B* **54** (1996) 17 884.